2026 IEEE International Conference on Robotics and Automation (ICRA 2026)
June 1-5, 2026. Vienna, Austria

Turning Disturbances into Actuation: Hierarchical Environment-Assisted MPC for USV Fault Recovery

Yang Hu[1], Sara Aldhaheri[1,2], Yanchao Wang[1], Peng Wu[1], and Yuanchang Liu[1,*]

***Abstract*— Thruster failures in unmanned surface vehicles (USVs) can critically compromise mission completion, particularly when severe degradation eliminates controllability in essential degrees of freedom. While traditional fault-tolerant control treats environmental disturbances as impediments to be rejected, this paper presents a novel approach: strategically exploiting wind and wave forces as virtual actuators for emergency harbor return. The proposed environment-assisted model predictive control (EAMPC) framework adaptively modulates environmental force utilization factors based on fault severity and the environmental force prediction confidence, transforming natural disturbances into environmental assistance. The hierarchical architecture integrates state estimation and prediction with physics-informed learning for short-term environmental forces, and reachability-based trajectory planning that exploits environmental forces to expand feasible zones. Theoretical analysis establishes practical input-to-state stability with explicit bounds quantifying degradation. Extensive validation across 320 trials demonstrates 91.25% mission success under 95% thruster degradation compared to 0% for baseline methods. This work demonstrates that strategic environmental exploitation fundamentally transforms fault recovery capabilities in marine robotics.**

I. INTRODUCTION

Unmanned surface vehicles (USVs) operating in maritime environments face a fundamental challenge: thruster failures can render them uncontrollable, leading to mission abort, asset loss, or collision hazards. Conventional fault-tolerant control methods for marine robots primarily rely on redistributing control effort among remaining actuators while rejecting environmental disturbances as adversarial effects [1], [2]. These approaches prove effective when vehicles possess redundant actuation or experience only moderate degradation. However, twin-thruster USVs, common in commercial and research applications, already operate with minimal control authority, unable to generate independent forces in all degrees of freedom. When severe thruster degradation occurs, these USVs lack sufficient actuation to maintain even basic controllability, resulting in mission failure.

This paper presents a paradigm shift: instead of rejecting environmental forces while struggling with insufficient actuation, the proposed approach strategically exploits wind and wave forces as virtual actuators to restore control authority. By transforming disturbances from adversaries into allies, the system maintains operational capability despite severe actuator degradation.

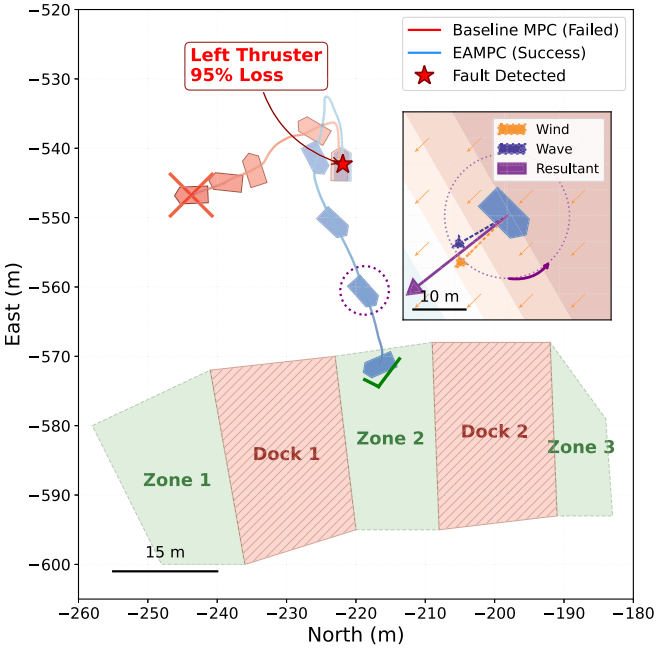

Fig. 1: Trajectories under 95% left thruster degradation: baseline MPC fails and drifts (red), while EAMPC successfully exploits environmental forces to reach the harbor (blue).

Consider a twin-thruster USV operating in open water when the left thruster suffers 95% degradation due to fouling or mechanical failure. As illustrated in Figure 1, this actuator loss creates a critical under-actuation scenario where baseline model predictive control (MPC) cannot maintain control authority with the remaining thrust capacity. Following fault detection, the USV must execute an emergency return to the nearest harbor zone. The red trajectory shows the baseline controller's failure as unable to compensate for the asymmetric thrust, the USV drifts away from the harbor, resulting in mission abort. However, the environmental forces present in the operating area represent untapped control authority. The proposed environment-assisted MPC (EAMPC) framework strategically harnesses these wind and wave forces, transforming them from disturbances into virtual actuators. By adaptively modulating the utilization of environmental forces through the reconfigured control allocation, EAMPC maintains trajectory tracking and successfully guides the USV to harbor zone without collision with dock areas.

Despite the clear potential for the exploitation poten-

[1]Department of Mechanical Engineering, University College London, London, United Kingdom. Emails: {yang.hu.24, sara.aldhaheri.22, yanchao.wang.20, wu.peng, yuanchang.liu*}@ucl.ac.uk
[2]Technology Innovation Institute, Abu Dhabi, United Arab Emirates.
*Corresponding author.
This work was supported by the Engineering and Physical Sciences Research Council (EPSRC) under Grant EP/Y000862/1, MarRI-UK, and Lloyd's Register.

tial illustrated above, existing approaches to environmental forces in marine robotics haven't explored this strategy. Environmental forces in marine robots have traditionally been addressed through two distinct strategies, neither of which considers them as replacement actuators. The dominant approach treats wind and wave forces as disturbances requiring rejection. Recent advances in adaptive neural coordinated control [3] and sliding mode techniques [4] demonstrate sophisticated methods to eliminate environmental perturbations, achieving precise tracking ability. However, these rejection-based strategies inherently assume sufficient control authority exists to counteract disturbances—an assumption that fails catastrophically when severe actuator degradation occurs. A second, emerging strategy seeks to exploit environmental forces for improved efficiency rather than control authority. Energy-aware path planning methods [5] and ocean current-assisted navigation strategies [6] leverage environmental dynamics to reduce fuel consumption and extend operational range. Yet these approaches optimize trajectories while still requiring fully functional actuators for control execution, offering no recourse when actuators fail. This critical gap, specifically the absence of methods that transform environmental forces into replacement actuators, motivates the proposed virtual actuator framework.

Unlike ground vehicles constrained by discrete friction or aerial vehicles facing rapid turbulence, USVs interact with wind and wave fields exhibiting sufficient temporal correlation for control exploitation. Modern USVs already estimate these forces through learning-based methods [7], [8], making the challenge not perfect prediction but robust utilization of available environmental authority.

This paper makes four key contributions toward hierarchical environment-assisted control framework: (i) formalization of virtual actuators through augmented control authority, proving that partial environmental utilization restores rank-deficient control matrices; (ii) environment-assisted MPC with confidence-aware utilization factors that scale with fault severity and prediction reliability, coupled with reachability-based planning that exploits environmental forces to expand feasible zones; (iii) practical input-to-state stability (ISS) guarantees with explicit bounds quantifying performance degradation under faults; and (iv) extensive validation demonstrating 91.25% mission success under 95% thruster degradation where conventional methods completely fail, while maintaining 20 Hz real-time execution.

This work enables autonomous USVs to operate beyond traditional safety margins in remote areas where recovery is impossible [9], [10], transforming environmental forces from threats into backup control mechanisms, fundamentally expanding the operational envelope of marine autonomy.

II. Problem Formulation

When a twin-thruster USV experiences severe actuator degradation, traditional fault-tolerant control methods fail due to insufficient control authority for trajectory tracking. However, the same environmental forces that challenge navigation, like wind and waves, can potentially be exploited as virtual actuation sources. This section formulates the control problem that transforms these disturbances into virtual actuators.

A. System Model and Fault Characterization

A medium-sized USV equipped with differential thrusters is considered, typical of vessels used for harbor surveillance and inspection tasks. Following Fossen's model of marine craft [11], the 3-DOF dynamics of the USV in the horizontal plane are:

$$\begin{aligned} \dot{\boldsymbol{\eta}} &= \mathbf{R}(\psi)\boldsymbol{\nu} \\ \mathbf{M}\dot{\boldsymbol{\nu}} + \mathbf{C}(\boldsymbol{\nu})\boldsymbol{\nu} + \mathbf{D}(\boldsymbol{\nu})\boldsymbol{\nu} &= \boldsymbol{\tau}_u + \mathbf{w} \end{aligned} \tag{1}$$

where $\boldsymbol{\eta} = [x, y, \psi]^T$ is the pose in earth-fixed frame, $\boldsymbol{\nu} = [u, v, r]^T$ denotes body-fixed velocities, and $\mathbf{R}(\psi)$ is the transformation matrix. The complete state vector is $\mathbf{x} = [\boldsymbol{\eta}^T, \boldsymbol{\nu}^T]^T \in \mathbb{R}^6$. The system matrices are: $\mathbf{M} \in \mathbb{R}^{3\times3}$ representing the system inertia matrix including added mass, $\mathbf{C}(\boldsymbol{\nu}) \in \mathbb{R}^{3\times3}$ capturing Coriolis and centripetal forces, and $\mathbf{D}(\boldsymbol{\nu}) \in \mathbb{R}^{3\times3}$ modeling hydrodynamic damping, and $\mathbf{w} = [w_x, w_y, w_\psi]^T$ representing the body-fixed bounded environmental forces acting on the USV. The control inputs produced by thrusters are:

$$\boldsymbol{\tau}_u = \mathbf{B}\mathbf{H}\mathbf{u}, \quad \mathbf{B} = \begin{bmatrix} 1 & 1 \\ 0 & 0 \\ -l/2 & l/2 \end{bmatrix} \tag{2}$$

where $\mathbf{u} = [T_1, T_2]^T$ are thruster commands (port and starboard respectively), $\mathbf{H} = \mathrm{diag}(h_1, h_2)$ with $h_i \in [0,1]$ for $i \in \{1,2\}$ represents health status, and l is the thruster separation distance. The matrix $\mathbf{B}$ reflects the differential thruster configuration: both thrusters contribute to forward thrust (first row), neither provides direct lateral force (second row), and they create opposing yaw moments (third row) with moment arm $l/2$.

Assumption 1. Thruster faults are abrupt and permanent: $h_i(t) = h_i^0$ for $t < t_f$ and $h_i(t) = h_i^f \in [0, h_i^0]$ for $t \geq t_f$, where t_f denotes fault occurrence time. Environmental forces satisfy $\|\mathbf{w}\| \leq w_{\max}$.

B. Controllability Analysis Under Faults

Lemma 1 (Post-Fault Controllability Loss)**.** *For single thruster failure (e.g., $h_1 = 0$), the system loses controllability with rank$(\mathbf{BH}) = 1 < 2$. Specifically:*

- *No lateral (sway) control: $\tau_y = 0$ always*
- *Coupled surge-yaw: $\tau_x = T_2$, $\tau_\psi = \frac{l}{2}T_2$ are locked in fixed ratio*
- *Lost direction: Cannot generate clockwise moments*

C. Virtual Actuator Framework

To recover controllability, partial environmental forces are introduced as virtual actuators:

Definition 1 (Augmented Control Authority)**.** *The effective control with environmental assistance is:*

$$\boldsymbol{\tau}_{eff} = \mathbf{B}\mathbf{H}\mathbf{u} + diag(\boldsymbol{\alpha})\mathbf{w} \tag{3}$$

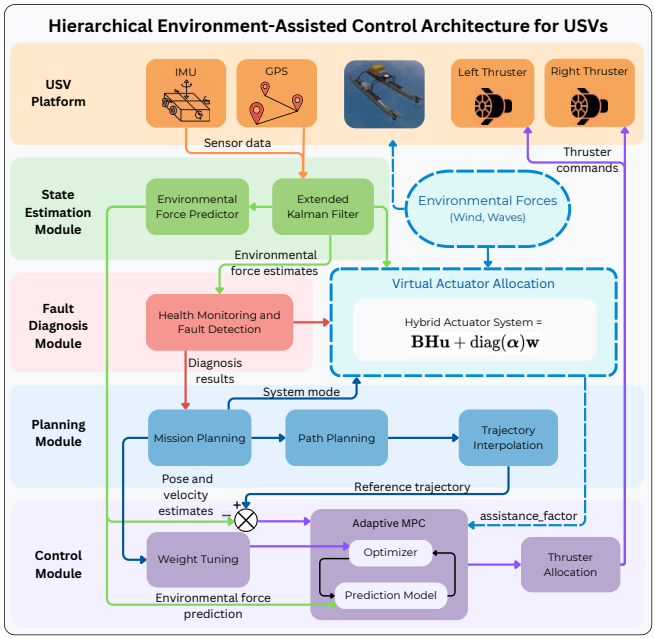

Fig. 2: Hierarchical environment-assisted control architecture. The Virtual Actuator Allocation module (blue dashed box) enables hybrid actuation through adaptive environmental force utilization based on fault severity.

where $\boldsymbol{\alpha} = [\alpha_x, \alpha_y, \alpha_\psi]^T \in [0,1]^3$ *serves as the controllable utilization factor. While the environmental forces* $\mathbf{w}$ *remain uncontrollable exogenous variables,* $\boldsymbol{\alpha}$ *represents the active decision variable within the control allocation that determines the proportion of available environmental force admitted into the system's effective control authority.*

The control problem becomes:

$$\min_{\mathbf{u}} \quad J = \int_0^{T_f} \left[\|\boldsymbol{\eta} - \boldsymbol{\eta}_{\text{ref}}\|^2_{\mathbf{Q}} + \|\mathbf{u}\|^2_{\mathbf{R}(\mathbf{H})} + \lambda(\mathbf{H})\|\boldsymbol{\alpha}\|^2 \right] dt \tag{4}$$

$$\text{s.t.} \quad \text{Dynamics (1)}, \quad \mathbf{x} \in \mathscr{X}, \quad \mathbf{u} \in \mathscr{U} \tag{5}$$

where $\mathbf{Q} = \text{diag}(q_x, q_y, q_\psi)$ weights position and heading tracking, $\mathbf{R}(\mathbf{H}) = \mathbf{R}_0 + \gamma \text{diag}(1-h_1, 1-h_2)$ adapts control penalty based on thruster health to discourage over-reliance on degraded actuators, $\lambda(\mathbf{H}) = \lambda_0 \cdot \frac{h_1+h_2}{2}$ penalizes environmental reliance proportional to fault severity, $\mathscr{U} = \{\mathbf{u} : 0 \le u_i \le u_{\max}, i \in \{1,2\}\}$ represents thrust constraints, and $\mathscr{X}$ denotes system state constraints. The utilization factors $\boldsymbol{\alpha}$ are determined by an adaptive policy (detailed in Section III) that ensures environmental forces augment control authority in the null space of $\mathbf{BH}$.

III. Hierarchical Control Architecture

The proposed architecture transforms environmental forces from disturbances to actuators through three key mechanisms: estimating current forces, predicting future forces, and optimally blending them with remaining thrust. It operates across three hierarchical layers as illustrated in Figure 2. The fault diagnosis algorithm is established based on [12].

Algorithm 1 Hierarchical Control Framework

Input: Initial state $\mathbf{x}_0$, goal position $\mathbf{x}_{\text{goal}}$
Output: Control commands $\mathbf{u}(t)$
while mission not complete **do**
  /* Monitor System Health (Event-triggered) */
  Detect thruster status $\mathbf{H} = \text{diag}(h_1, h_2)$
  if fault detected **then**
    Enable environmental assistance: $\boldsymbol{\alpha} > 0$
    Set replan flag $\leftarrow$ true
  end if
  /* Estimate Environmental Forces (100 Hz) */
  Update state and force estimates: $[\hat{\mathbf{x}}, \hat{\mathbf{w}}] \leftarrow \text{EKF}$
  Learn force patterns: $\boldsymbol{\Theta} \leftarrow \text{RLS}(\hat{\mathbf{w}})$
  Predict future forces: $\{\hat{\mathbf{w}}_k\}_{k=1}^N \leftarrow \boldsymbol{\Theta}^T \bar{\boldsymbol{\phi}}$
  /* Mission Planning (2 Hz) */
  if replan flag **or** $\|\mathbf{x} - \mathbf{x}_{\text{ref}}\| > d_{\text{thresh}}$ **then**
    Select safe harbor zone: $z^* \leftarrow \text{evaluateZones}(\hat{\mathbf{x}}, \hat{\mathbf{w}}, \mathbf{H})$
    Generate trajectory: $\mathbf{x}_{\text{ref}} \leftarrow \text{planPath}(\mathbf{x}, z^*, \hat{\mathbf{w}})$
  end if
  /* Environment-Assisted Control (20 Hz) */
  Compute utilization: $\boldsymbol{\alpha} \leftarrow f(\mathbf{H}, \sigma_\Theta)$ via Eq. (8)
  Solve MPC with hybrid actuation:
    $\mathbf{u}^* \leftarrow \arg\min J$ s.t. $\boldsymbol{\tau} = \mathbf{BHu} + \text{diag}(\boldsymbol{\alpha})\hat{\mathbf{w}}$
  Apply control: $\mathbf{u}(t) = \mathbf{u}_0^*$
end while
return Mission success

Upon fault detection, the system transitions from conventional thruster-based control to hybrid actuation mode, where environmental forces supplement degraded thrust capacity. The framework comprises: (i) a disturbance observer using Extended Kalman Filter (EKF) for real-time environmental force estimation, with a data-driven predictor that learns force patterns for multi-step predictions, (ii) the proposed EAMPC that modulates environmental force utilization based on fault severity and prediction confidence, and (iii) a high-levels planner that generates feasible trajectories considering reduced control authority. The Virtual Actuator Allocation module synthesizes hybrid actuation by combining degraded thruster forces with environmental assistance. Prediction confidence and fault severity determine the utilization factors $\boldsymbol{\alpha}$, while environmental forces over the prediction horizon are incorporated directly into the MPC model.

Algorithm 1 presents the overall control flow, showing the interaction between fault monitoring, state estimation, planning, and control layers.

A. Environment-Assisted MPC

1) Disturbance Observer: An Extended Kalman Filter estimates the augmented state $\mathbf{x}_a = [\boldsymbol{\eta}^T, \boldsymbol{\nu}^T, \mathbf{w}^T]^T$ with process model:

$$\dot{\mathbf{x}}_a = \begin{bmatrix} \mathbf{R}(\psi)\boldsymbol{\nu} \\ \mathbf{M}^{-1}(\boldsymbol{\tau}_u + \mathbf{w} - \mathbf{C}\boldsymbol{\nu} - \mathbf{D}\boldsymbol{\nu}) \\ \mathbf{0} \end{bmatrix} + \begin{bmatrix} \mathbf{0} \\ \mathbf{0} \\ \boldsymbol{\xi}_w \end{bmatrix}, \boldsymbol{\xi}_w \sim \mathscr{N}(\mathbf{0}, \mathbf{Q}_w) \tag{6}$$

where disturbances evolve as a random walk with tunable covariance $\mathbf{Q}_w$.

2) Data-Driven Environmental Prediction: To enable predictive control, a recursive least squares (RLS) is employed with physics-informed features. The parameter matrix $\boldsymbol{\Theta}(t) \in \mathbb{R}^{7\times 3}$ maps normalized features to forces:

$$\hat{\mathbf{w}}(t+\tau) = \boldsymbol{\Theta}^T(t)\bar{\boldsymbol{\phi}}(t,\tau) \tag{7}$$

where $\hat{\mathbf{w}}(t+\tau) \in \mathbb{R}^3$ represents the predicted environmental forces at time $t+\tau$, and the feature vector $\bar{\boldsymbol{\phi}}(t,\tau) \in \mathbb{R}^7$ contains normalized physics-informed features: mean force magnitude $\|\mathbf{w}\|_{\text{avg}}$, dominant frequency f_{dom} from spectral analysis, force variance σ_w^2, temporal evolution rates $\dot{w}_x, \dot{w}_y, \dot{w}_\psi$ capturing directional force dynamics, and phase predictor $\cos(2\pi f_{\text{dom}}\tau + \hat{\varphi})$ for oscillatory patterns.

The RLS update with forgetting factor $\lambda \in [0.95, 1)$ follows standard formulation with covariance $\mathbf{P} \in \mathbb{R}^{7\times 7}$ and gain $\mathbf{K} \in \mathbb{R}^{7\times 1}$.

Assumption 2 (Natural Excitation). Environmental forces exhibit sufficient richness: $\lambda_{\min}(\mathbb{E}_T[\bar{\boldsymbol{\phi}}\bar{\boldsymbol{\phi}}^T]) \geq \beta > 0$ over window $T \geq 20$s, with $\beta \geq 0.05$ for Sea States 2-5. This ensures environmental forces contain enough variation for reliable parameter learning without requiring artificial excitation signals.

Remark 1. This assumption holds naturally in marine environments due to wave periodicity and wind gusts. The threshold $\beta = 0.05$ corresponds to environmental variations of at least 10% of mean values, easily satisfied except in glassy calm conditions.

3) Confidence-Aware Assistance Policy: The key innovation is adaptive modulation of environmental utilization based on fault severity and prediction confidence. The assistance factor determines how much predicted environmental force is incorporated into the control strategy, and balances two competing objectives: exploiting environmental forces for control (higher α) versus robustness to prediction errors (lower α):

$$\alpha(t) = \begin{cases} \min\left\{1, \frac{\kappa}{\sigma_\Theta(t)+\varepsilon}\right\} \cdot \mu(\mathbf{H}) & \text{if fault detected} \\ 0 & \text{otherwise} \end{cases} \tag{8}$$

where $\alpha \in [0,1]$ is the environmental utilization factor, $\kappa = 1.5$ is a tuning parameter, $\varepsilon = 0.01$ prevents numerical instability, and $\sigma_\Theta(t) = \|\mathbf{P}(t)\|_F$ aggregates uncertainty across all parameter estimates, providing a scalar confidence metric. The fault severity function $\mu(\mathbf{H})$ maps thruster health to required assistance level:

$$\mu(\mathbf{H}) = \begin{cases} 0 & \text{if } h_1 + h_2 > 1.8 \\ 1 - \frac{h_1+h_2}{2} & \text{if } 0.4 \leq h_1 + h_2 \leq 1.8 \\ 1 & \text{if } h_1 + h_2 < 0.4 \end{cases} \tag{9}$$

where thresholds correspond to operational modes: normal operation (combined health $>$ 90%), degraded operation (20%-90%), and critical failure ($<$ 20% capacity). This formulation ensures: (i) no environmental assistance for minor degradation where thrusters remain sufficient, (ii) progressive assistance as faults worsen, and (iii) maximum environmental exploitation under critical failures. As prediction confidence increases (σ_Θ decreases), the system more aggressively utilizes environmental forces, while maintaining robustness through the saturation bound. This policy enables smooth transition from traditional thrust-based control to environment-assisted operation as actuator health degrades.

4) MPC Formulation with Guaranteed Feasibility: The MPC with horizon N solves:

$$\min_{\mathbf{U}} \quad \sum_{k=0}^{N-1} \ell(\mathbf{x}_k, \mathbf{u}_k) + V_f(\mathbf{x}_N) \tag{10a}$$

$$\text{s.t.} \quad \mathbf{x}_{k+1} = f_d(\mathbf{x}_k, \boldsymbol{\tau}_k) \tag{10b}$$

$$\boldsymbol{\tau}_k = \mathbf{B}\mathbf{H}\mathbf{u}_k + \alpha_k \hat{\mathbf{w}}_k \tag{10c}$$

$$\mathbf{u}_k \in [0, u_{\max}]^2, \quad \mathbf{x}_k \in \mathscr{X} \tag{10d}$$

$$\mathbf{x}_N \in \mathscr{X}_f \tag{10e}$$

where $\mathbf{U} = \{\mathbf{u}_0, \mathbf{u}_1, \ldots, \mathbf{u}_{N-1}\}$ denotes the control sequence, $\ell(\mathbf{x}_k, \mathbf{u}_k) = \|\mathbf{x}_k - \mathbf{x}_{\text{ref},k}\|_{\mathbf{Q}}^2 + \|\mathbf{u}_k\|_{\mathbf{R}(\mathbf{H})}^2$ is the stage cost, and f_d represents the discretized dynamics. The terminal set $\mathscr{X}_f$ is the maximal robust control invariant set with terminal cost $V_f(\mathbf{x}) = \|\mathbf{x} - \mathbf{x}_{\text{ref},N}\|_{\mathbf{P}_f}^2$, where $\mathbf{P}_f$ solves the discrete-time algebraic Riccati equation.

Lemma 2 (Recursive Feasibility)**.** *If* (10) *is feasible at time t and $\|\hat{\mathbf{w}}_k - \mathbf{w}_k\| \leq \delta_w$ for all k, then it remains feasible at $t+1$ with candidate solution $\tilde{\mathbf{U}}_{t+1} = \{\mathbf{u}_1^*, \ldots, \mathbf{u}_{N-1}^*, \kappa_f(\mathbf{x}_N^*)\}$, where $\kappa_f : \mathscr{X}_f \to \mathscr{U}$ is the terminal controller associated with $\mathscr{X}_f$.*

B. Reachability-Based Planning

While the EAMPC ensures local trajectory tracking, safe mission completion requires high-level planning that accounts for reduced control authority. This section presents a hierarchical planning framework that generates feasible reference trajectories by exploiting environmental forces to expand the reachable set.

1) Impact of Thruster Failure on Reachability: Single thruster failure fundamentally alters the USV's motion capabilities. Consider a starboard thruster failure, the USV loses symmetric control authority. The remaining port thruster generates coupled forward thrust and counter-clockwise yaw moment ($M_z = -\ell T_1/2$), making straight-line motion impossible without environmental assistance. The USV has no lateral control and cannot produce clockwise rotation.

The time-varying reachable set under environmental assistance is:

$$\mathscr{R}_t(\mathbf{x}_0, \mathbf{H}) = \{\mathbf{x}_f : \exists \mathbf{u}(\cdot), \alpha(\cdot) \text{ s.t. } \mathbf{x}(t) = \mathbf{x}_f, \mathbf{x}(0) = \mathbf{x}_0\} \tag{11}$$

where evolution follows dynamics (1) with $\mathbf{u} \in \mathscr{U}$ and $\mathbf{x}_f$ denotes final state. The reachable set is constrained by both remaining control authority and available environmental assistance, creating asymmetric reachability regions favoring directions aligned with environmental forces. For example, with only port thruster available ($h_2 = 0$), the USV can only reach points in the port-forward quadrant without assistance. However, with tailwind assistance ($\alpha_x w_x > 0$), previously unreachable straight-ahead positions become feasible.

2) Adaptive Zone Selection Strategy: The planner maintains safe harbor zones $\mathscr{Z} = \{z_1, z_2, \ldots, z_m\}$ and solves:

$$z^* = \arg\min_{z \in \mathscr{Z}} J_{\text{plan}}(z) \tag{12}$$

subject to collision-free path constraints and $\mathbf{x}_z \in \mathscr{R}_{T_{\max}}(\mathbf{x}_0, \mathbf{H})$, where $\mathbf{x}_z$ denotes the target zone position.

The cost function J_{plan} balances three factors: normalized distance to zone, environmental force alignment, and zone commitment stability. The environmental alignment quantifies how predicted forces assist motion toward each zone through the dot product between force and desired direction vectors. To prevent oscillatory switching, the hysteresis-based commitment mechanism is implemented that increases selection persistence as distance decreases. Figure 3 shows the iterative replanning process for emergency harbor return under severe (95%) left thruster failure.

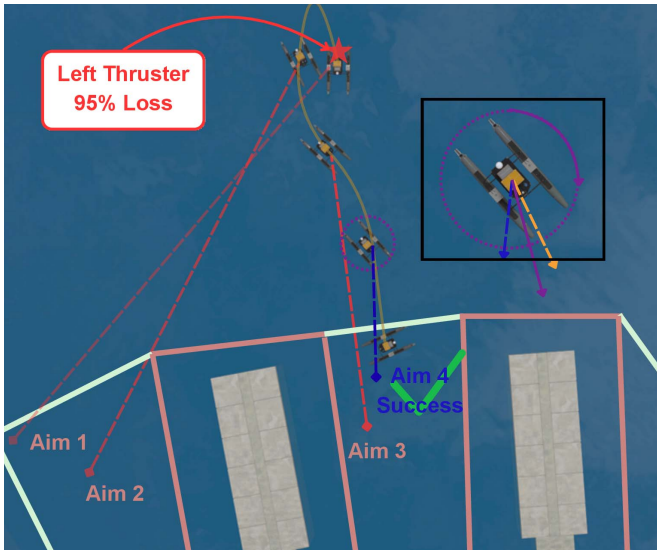

Fig. 3: Evolution of reachability-based trajectory planning. Red paths show replanned trajectories as the system refines environmental force predictions, while the final blue trajectory demonstrates successful harbor return through reachability enhanced by beneficial environmental forces.

3) Trajectory Generation and MPC Interface: Once a target zone is selected, the planner generates energy-optimal reference trajectories:

$$\mathbf{x}_{\text{ref}}^* = \arg\min_{\mathbf{x}(\cdot)} \int_0^{T_h} \|\mathbf{u}\|^2_{\mathbf{R}(\mathbf{H})} dt \tag{13}$$

subject to dynamics, collision avoidance, and terminal constraints $\mathbf{x}(T_h) = \mathbf{x}_z$, where T_h is the planning horizon.

This formulation naturally produces trajectories leveraging environmental assistance while minimizing thruster effort. The planning-MPC interface ensures stability through:

- **Feasibility margins**: Reference waypoints maintain minimum distance δ from all constraint boundaries
- **Event-triggered replanning**: Updates occur only when environmental changes exceed the threshold σ_w or tracking errors exceed $\varepsilon_{\text{track}}$
- **Continuity constraints**: Smooth transitions limit reference discontinuities to $\|\Delta\mathbf{x}_{\text{ref}}\| \leq \rho_{\text{cont}}$

IV. Stability Analysis

The practical ISS property guarantees that tracking errors remain bounded despite permanent actuator faults and environmental prediction errors. Unlike asymptotic stability, practical ISS accepts a small steady-state error d_{ult} in exchange for robustness to model uncertainty.

A. Main Result

Theorem 1 (Practical Input-to-State Stability)**.** *Under Assumption 2, the tracking error $\mathbf{e} = \mathbf{x} - \mathbf{x}_{ref}$ is practically ISS with respect to estimation error $\mathbf{e}_w = \mathbf{w} - \hat{\mathbf{w}}$:*

$$\|\mathbf{e}(k)\| \leq \beta_e(\|\mathbf{e}(0)\|, k) + \gamma_e\left(\sup_{j \leq k} \|\mathbf{e}_w(j)\|\right) + d_{ult} \tag{14}$$

where $\beta_e \in \mathscr{K}\mathscr{L}$, $\gamma_e \in \mathscr{K}$, and the ultimate bound:

$$d_{ult} = \sqrt{\frac{2tr(\mathbf{Q}_w)}{\lambda_{\min}(\mathbf{Q})(1-\lambda)\beta}} + \frac{L_w w_{\max}}{\lambda_{\min}(\mathbf{Q})} \cdot \mu(\mathbf{H}) \tag{15}$$

with L_w the Lipschitz constant of environmental forces, λ the RLS forgetting factor, β the excitation level from Assumption 2, and degradation factor $\mu(\mathbf{H}) = (3 - rank(\mathbf{BH}))/3 \in [0,1]$ quantifying controllability loss.

Remark 2 (Physical Interpretation). The ultimate bound consists of two terms: the first captures uncertainty from environmental force variations ($\mathbf{Q}_w$), while the second, scaled by $\mu(\mathbf{H})$, represents error due to lost control directions. For healthy thrusters ($\mu = 1/3$), the bound is minimal; for single failure ($\mu = 2/3$), it doubles; for complete failure ($\mu = 1$), the bound reaches its maximum.

Proof Sketch. Construct composite Lyapunov function:

$$V(k) = V^*(\mathbf{e}(k)) + \gamma \text{tr}(\tilde{\mathbf{\Theta}}^T \mathbf{P}^{-1} \tilde{\mathbf{\Theta}}) \tag{16}$$

where $\tilde{\mathbf{\Theta}} = \mathbf{\Theta} - \mathbf{\Theta}^*$ is the parameter estimation error and $\gamma = L_w^2/(\lambda\beta\lambda_{\min}(\mathbf{Q}))$.

The proof combines two stability arguments: V^* ensures MPC tracking stability, while the second term bounds parameter estimation error. By recursive feasibility (Lemma 2) and optimality:

$$V^*(k+1) - V^*(k) \leq -\lambda_{\min}(\mathbf{Q})\|\mathbf{e}(k)\|^2 + L_w\|\mathbf{e}_w(k)\| \tag{17}$$

Under Assumption 2, the parameter error satisfies:

$$\mathbb{E}[\|\tilde{\mathbf{\Theta}}(k+1)\|_P^2] \leq (1-\lambda\beta)\|\tilde{\mathbf{\Theta}}(k)\|_P^2 + \frac{\text{tr}(\mathbf{Q}_w)}{1-\lambda} \tag{18}$$

where $\|\cdot\|_P^2 = (\cdot)^T \mathbf{P}^{-1}(\cdot)$. The degradation factor $\mu(\mathbf{H})$ captures uncontrollable directions due to faults. Combining these yields the stated ISS property.

B. Convergence and Robustness

Corollary 1 (Parameter Convergence)**.** *The RLS estimation error converges exponentially:*

$$\limsup_{k\to\infty} \mathbb{E}[\|\tilde{\boldsymbol{\Theta}}(k)\|_F^2] \leq \frac{tr(\mathbf{Q}_w)}{(1-\lambda)\beta} \tag{19}$$

Corollary 2 (Detection Delay Tolerance)**.** *The system remains stable if detection delay $\tau_d < \bar{\tau}_d$, where:*

$$\bar{\tau}_d = \inf\{t : \mathscr{R}_t(\mathbf{x}_0) \cap \partial\mathscr{X}_{safe} \neq \emptyset\} \tag{20}$$

is the time until the degraded reachable set intersects safety boundaries.

V. Experimental Validation

The proposed environment-assisted control framework is validated through extensive simulations in the Virtual RobotX (VRX) maritime environment [13].

A. Experimental Setup

Experiments are conducted using the VRX simulator in Gazebo with the WAM-V USV model. The simulator incorporates realistic hydrodynamic forces, thruster dynamics, and environmental disturbances based on the Gazebo physics engine. To comprehensively evaluate the proposed method under varying operational scenarios, multiple experiments are performed across a range of sea states and directional configurations.

1) Environmental Conditions: Experiments are conducted across Sea States 2-5 as Table I. These conditions span the operational envelope from routine operations (Sea State 2-3) to challenging scenarios (Sea State 4-5).

TABLE I: Environmental Test Conditions

Sea State	Wind (m/s)	Wave Height (m)	Period (s)	Condition
2 (Smooth)	3-4	0.2-0.4	3-4	Routine
3 (Slight)	5-7	0.5-0.8	4-5	Routine
4 (Moderate)	8-10	0.9-1.3	5-6	Challenging
5 (Rough)	11-13	1.4-2.0	6-7	Emergency

Performance across varying environmental alignments was assessed through multiple directional configurations. The **beneficial configuration** aligns environmental forces with harbor approach: wind from 160°–200° generates northward assistance, while waves from 150°–190° create constructive yaw moments through force misalignment. The **nominal configuration** represents challenging operational conditions: quartering seas with wind from 110°–145° and waves from 95°–120° producing strong lateral forces.

2) Fault Scenarios: Permanent thruster faults are injected at $t = 15$ s during mission execution across three severity levels: **moderate degradation** (50%, $h_i = 0.5$) maintains partial controllability, **severe degradation** (75%, $h_i = 0.25$) causes significant control authority loss, and **critical degradation** (95%, $h_i = 0.05$) represents near-complete actuator failure. Each configuration undergoes testing with multiple random seeds for environmental variability. Mission success requires reaching within 0.5 m of any harbor zone within 180 s post-fault while avoiding collision with dock areas.

3) Implementation Details: Both the baseline MPC and proposed EAMPC employ identical configurations to ensure fair comparison: hierarchical control at 2 Hz (planning), 20 Hz (MPC), and 100 Hz (state estimation). The MPC uses horizon $N = 60$ with sampling time $T_s = 0.05$ s, solved via ACADOS [14]. The sole difference lies in the environmental force utilization: baseline MPC treats $\mathbf{w}$ as disturbances to reject, while EAMPC incorporates them as virtual actuators. Both controllers use identical cost weights $\mathbf{Q} = \text{diag}(80, 10, 150, 5, 5, 5)$ and $\mathbf{R} = \text{diag}(0.001, 0.001)$ prior to fault-adaptive adjustment.

B. Results and Discussion

Analysis of 320 trials (240 across 50%–95% degradation, 80 edge cases with complete failure) in Sea States 2–5 reveals how environmental forces fundamentally transform from control challenges into actuation as thruster capacity diminishes. Across all trials, the minimum eigenvalue of the feature correlation matrix $\mathbb{E}_T[\bar{\boldsymbol{\phi}}\bar{\boldsymbol{\phi}}^T]$ remained above 0.08, confirming that Assumption 2 holds in practice for Sea States 2-5. The proposed EAMPC and conventional MPC baseline underwent testing under equivalent harbor return scenarios, with computational performance averaging 12.3 ms per optimization cycle, satisfying real-time constraints for 20 Hz control execution. The following analysis examines system performance through comparative control results, quantitative performance metrics across fault severities, and operational envelope characterization.

1) Comparative Performance Under Fault Conditions: Figure 4 demonstrates the fundamental advantage of environment-assisted control across two critical fault scenarios. Under moderate degradation (50%, top row), both methods successfully reach the harbor, but the proposed approach achieves 52% faster recovery (27.5s vs 57.3s) through strategic environmental force utilization, maintaining around 32% average environmental contribution post-fault. The stark contrast emerges under severe degradation (95%, bottom row): while baseline MPC experiences critical failure with uncontrolled drift, the proposed EAMPC maintains trajectory tracking by leveraging 65% environmental contribution, effectively transforming disturbances into primary actuation.

The control authority transition follows a clear pattern across degradation levels. At 50% degradation, the system operates in hybrid mode with thrusters providing primary control while environmental forces assist in correction. Comparatively, at 95% degradation, the relationship inverts completely: environmental forces become primary actuators while the minimal remaining thruster authority serves only to maintain differential balance for steering. This progressive transition from disturbance rejection to disturbance exploitation represents the core innovation enabling mission completion under severe faults.

2) Quantitative Performance Metrics: Table II quantifies performance across 240 fault scenarios. The proposed EAMPC maintains 100% success through 75% degradation, declining to 91.25% at 95%, while baseline MPC collapses

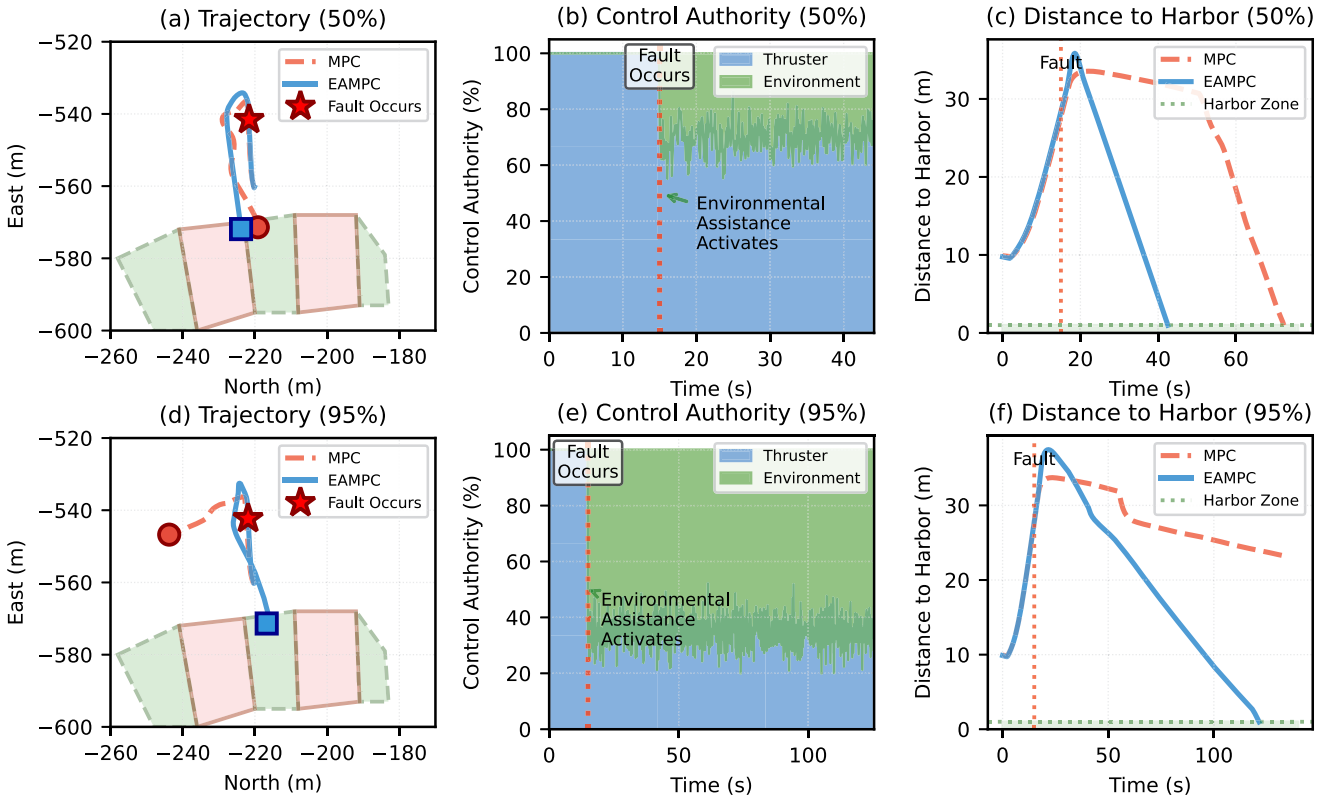

Fig. 4: Performance comparison between baseline MPC and the proposed EAMPC under 50% (top) and 95% (bottom) left thruster degradation. Fault occurs at $t = 15$ s. (a,d) Trajectory tracking, (b,e) Control authority distribution showing environmental force utilization, (c,f) Distance to harbor convergence. Under severe degradation (95%), only EAMPC maintains control through 65% environmental assistance while baseline MPC fails.

from 80% at 50% to 0% at 95%. This widening gap demonstrates environmental assistance transitioning from advantageous to essential as faults worsen.

Energy consumption unexpectedly decreases with fault severity, dropping from 109±14 kJ at 50% degradation to only 43±7 kJ at 95% degradation. At moderate faults, the system maintains dual-thruster operation with environmental augmentation, consuming substantial energy. At severe faults, heavy environmental reliance minimizes thruster use, with remaining authority serving primarily for differential balance. Path lengths correspondingly increase as the zone selection prioritizes environmental alignment over proximity under severe degradation.

3) Operational Envelope Analysis: Figure 5 maps the operational envelope across fault severity and sea state space, with an additional 80 edge cases testing complete thruster failure (100%). The proposed EAMPC maintains 100% success rates for moderate faults (50%-75%) across all sea conditions, demonstrating effective fault tolerance within the normal operational envelope. However, the behavior at extreme degradation (95%-100%) reveals a counterintuitive phenomenon: moderate sea conditions (State 4) provide better fault recovery than calm seas (State 2–3).

This inversion occurs because calm conditions fail to provide sufficient environmental excitation for the control algorithm to exploit. In Sea State 2, the system achieves only 15% success at 100% degradation, as weak environmental forces cannot compensate for complete thruster loss before the USV drifts beyond recovery. Conversely, Sea State 4 providing adequate forces for emergency return while remaining

TABLE II: Performance Metrics Across Fault Scenarios

Fault Type[a]	Environmental Conditions	Success Rate	Time to Harbor (s)	Energy (kJ)	Path Length (m)
EAMPC (Proposed)					
L95%	Beneficial	**20/20**	75±8	41±9	96
	Nominal	17/20	90±17	43±7	96
L75%	Beneficial	**20/20**	39±6	82±2	78
	Nominal	**20/20**	45±8	94±8	79
L50%	Beneficial	**20/20**	28±1	96±7	**68**
	Nominal	**20/20**	30±2	109±14	70
R95%	Beneficial	**20/20**	87±2	**37±11**	95
	Nominal	16/20	88±6	40±16	96
R75%	Beneficial	**20/20**	36±2	64±4	82
	Nominal	**20/20**	37±3	66±7	83
R50%	Beneficial	**20/20**	**27±2**	91±8	72
	Nominal	**20/20**	30±1	104±11	73
Baseline MPC (No Environmental Assistance)					
L/R 95%	Both	**0/20**	Failed	–	–
L/R 75%	Both	3/20	62±15	94±22	51
L/R 50%	Both	16/20	57±12	97±18	47

[a] L/R denotes Left/Right thruster; percentage indicates thrust degradation severity

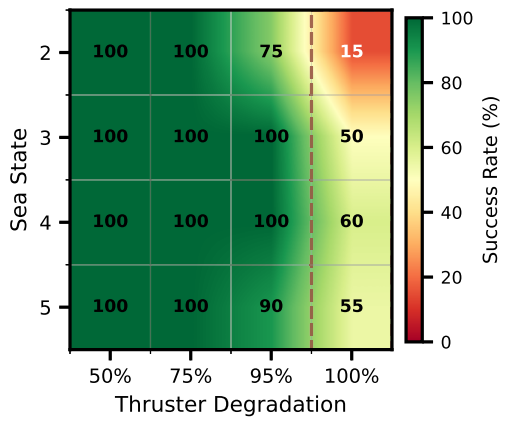

Fig. 5: Mission success rates of the EAMPC across varying sea states and thruster degradation levels. The system maintains operational capability (indicated by the dashed contour) under rough sea conditions with critical thruster degradation.

predictable enough for control.

This finding challenges conventional maritime wisdom that "calmer is safer." For the proposed environment-assisted system, the results demonstrate that moderate, predictable environmental force successfully enhance survivability by providing exploitable control authority when traditional actuation fails.

VI. Conclusion and Future Work

This paper presented a novel approach to environmental-assisted control that transforms disturbances from control challenges into exploitable actuation resources. The proposed EAMPC framework demonstrates that wind and wave forces, traditionally viewed as impediments, can restore control authority when actuators fail, fundamentally expanding the operational envelope of autonomous USVs.

The hierarchical architecture achieves this transformation through three integrated mechanisms. First, the formalization of virtual actuators proves that partial environmental utilization mathematically restores rank-deficient control matrices, recovering controllability in previously uncontrollable directions. Second, the confidence-aware utilization policy adaptively scales environmental force incorporation based on fault severity and prediction uncertainty, ensuring robust performance without external excitation. Third, reachability-based planning explicitly leverages environmental assistance to expand feasible mission zones, enabling successful harbor return despite severe degradation.

Theoretical analysis established practical ISS with explicit degradation bounds, guaranteeing bounded tracking error proportional to fault severity. The framework maintains stability under realistic detection delays and converges without artificial excitation, critical for practical deployment.

Experimental validation across 320 trials yielded compelling simulation results. The system achieved 91.25% mission success under 95% thruster degradation; these are conditions where conventional methods fail completely. Counterintuitively, moderate to rough sea conditions provided superior fault recovery compared to calm seas, as environmental forces must exceed a minimum threshold to enable virtual actuation. This finding challenges the traditional maritime assumption that calmer conditions are inherently safer.

Future work will pursue three directions: (i) sea trials on physical USV platforms to validate simulation results, (ii) extension to multi-fault scenarios including sensor degradation, and (iii) integration with deep learning for long-horizon environmental prediction.

References

[1] G. Zhang, S. Chu, W. Zhang, and C. Liu, "Adaptive neural fault-tolerant control for usv with the output-based triggering approach," *IEEE Transactions on Vehicular Technology*, vol. 71, no. 7, pp. 6948–6957, 2022.

[2] C. Liu, H. Chen, B. Jiang, Y. Zhang, and S. Xie, "Adaptive reconfigurable fault-tolerant control of multi-usvs with actuator magnitude and rate faults," *IEEE Transactions on Industrial Electronics*, vol. 72, no. 8, pp. 8512–8521, 2025.

[3] X. Hu, G. Zhu, Y. Ma, Z. Li, R. Malekian, and M. Á. Sotelo, "Dynamic event-triggered adaptive formation with disturbance rejection for marine vehicles under unknown model dynamics," *IEEE Transactions on Vehicular Technology*, vol. 72, no. 5, pp. 5664–5676, 2023.

[4] J. Guerrero, A. Chemori, V. Creuze, and J. Torres, "Improved adaptive high-order sliding mode-based control for trajectory tracking of autonomous underwater vehicles," *IEEE Journal of Oceanic Engineering*, vol. 49, no. 4, pp. 1337–1349, 2024.

[5] S. Zhang, H. Sang, X. Sun, F. Liu, Y. Zhou, and P. Yu, "A multi-objective path planning method for the wave glider in the complex marine environment," *Ocean Engineering*, vol. 264, p. 112481, 2022.

[6] J. Yang, J. Huo, M. Xi, J. He, Z. Li, and H. H. Song, "A time-saving path planning scheme for autonomous underwater vehicles with complex underwater conditions," *IEEE Internet of Things Journal*, vol. 10, no. 2, pp. 1001–1013, 2023.

[7] J. Martins, P. Pereira, R. Campilho, and A. Pinto, "Wave-motion compensation for usv–uav cooperation: A model predictive controller approach," in *2024 20th IEEE/ASME International Conference on Mechatronic and Embedded Systems and Applications (MESA)*, 2024, pp. 1–8.

[8] H. Luo, J. Ge, S. Qin, G. Hou, and S. Xu, "An extreme-short-term predicted model of the learning-based approach for multi-step usv maneuvering motions," *Ocean Engineering*, vol. 340, p. 122353, 2025.

[9] P. Dash, R. J. Moorhead, J. Herman, W. Beshah, M. S. Sankar, J. Moorhead, G. D. Chesser, W. Lowe, J. Simmerman, G. Turnage, A. P. Katkar, and J. P. Liles, "Evaluation of water quality data collected using a novel autonomous surface vessel," in *OCEANS 2021: San Diego – Porto*, 2021, pp. 1–10.

[10] R. Song, S. Gao, and Y. Li, "A novel approach to multi-usv cooperative search in unknown dynamic marine environment using reinforcement learning," *Neural Computing and Applications*, vol. 37, no. 21, pp. 16 055–16 070, 2025.

[11] T. I. Fossen, *Handbook of marine craft hydrodynamics and motion control*. John Wiley & Sons, 2011.

[12] Y. Hu, S. Aldhaheri, Y. Wang, P. Wu, and Y. Liu, "Enhancing human-robot trust and collaboration in unmanned surface vehicles through fault diagnosis," in *2025 34rd IEEE International Conference on Robot and Human Interactive Communication (ROMAN)*, 2025.

[13] B. Bingham, C. Agüero, M. McCarrin, J. Klamo, J. Malia, K. Allen, T. Lum, M. Rawson, and R. Waqar, "Toward maritime robotic simulation in gazebo," in *OCEANS 2019 MTS/IEEE SEATTLE*, 2019, pp. 1–10.

[14] R. Verschueren, G. Frison, D. Kouzoupis, J. Frey, N. v. Duijkeren, A. Zanelli, B. Novoselnik, T. Albin, R. Quirynen, and M. Diehl, "acados—a modular open-source framework for fast embedded optimal control," *Mathematical Programming Computation*, vol. 14, no. 1, pp. 147–183, 2022.